Journal of Alloys and Compounds 524 (2012) 38–45

Contents lists available at SciVerse ScienceDirect

Journal of Alloys and Compounds

journal homepage: www.elsevier.com/locate/jallcom

Phase diagram and thermodynamic properties of compounds of the AgI–TlI–I system

Mahammad B. Babanly[a,*], Leyla F. Mashadieva[a], Ziya S. Aliev[a], Andrei V. Shevelkov[b,**], Yusif A. Yusibov[a]

[a] Baku State University, General and Inorganic Chemistry Department, Azerbaijan
[b] Moscow Lomonosov State University, Chemistry Department, Russia

ARTICLE INFO

Article history:
Received 31 October 2011
Received in revised form 30 January 2012
Accepted 6 February 2012
Available online 16 February 2012

Keywords:
Silver-thallium iodides
Phase diagram
Phase equilibriums
Thermodynamics
Electro-motive force

ABSTRACT

The AgI–TlI–I system was investigated by a combination of DTA and XRD methods and EMF measurements with the Ag_4RbI_5 solid electrolyte. A series of polythermal sections and the projection of the liquidus surface were constructed. The fields of the primary crystallization and the types and coordinates of non- and monovariant equilibriums were determined. As a result, the self-consistent phase diagram of the AgI–TlI–I was drawn. The partial molar functions ($\Delta\bar{G}$, $\Delta\bar{H}$, $\Delta\bar{S}$) of silver iodide and silver in the alloys as well as the standard thermodynamic functions of formation and the standard entropies of $AgTl_3I_5$, $AgTl_2I_3$, and $AgTlI_2$ were calculated from the EMF measurements.

1. Introduction

Complex silver iodides are a vast family of compounds having different crystal structures and properties. Many of them are superionic conductors, possessing high Ag^+ conductivity. They include ternary iodides such as Ag_4RbI_5 and Ag_2HgI_4, chalcogenide-iodides exemplified by Ag_3SI, and complex salts like $Ag_4I(PO_4)$. Many of these compounds are used as ion-selective electrodes, solid-state electrolytes in the different kind of electric batteries, sensors, displays, etc. [1–5]. The search for new multicomponent silver iodides and nonstoichiometric phases on their base as well as creation of new methods for their synthesis are the hot topics, which require detailed investigation of phase equilibriums in the corresponding systems.

Silver-thallium ternary iodides belong to the family of complex silver iodides. There are three phases reported to exist in the Ag–Tl–I system, $AgTl_2I_3$, $AgTlI_2$, and $AgTl_3I_5$, with the two former belonging to the AgI–TlI quasi-binary subsystem. $AgTl_2I_3$ crystallizes in the trigonal system, space group *R*-3*m*, with the unit cell parameters a = 10.443 and c = 19.935 Å [6], $AgTlI_2$ has a tetragonal crystal structure, space group *I*4/*mcm*; a = 8.34; c = 7.66 Å [7], and $AgTl_3I_5$ crystallizes in the hexagonal system, space group *P*-62*c*, with the unit cell parameters a = 10.480; c = 13.415 Å [8]. Their crystal structures are different; however, they can be described in a similar manner, emphasizing the coordination polyhedra of silver. Fig. 1 shows that the crystal structure of $AgTlI_2$ features columns of the edge-sharing tetrahedra running along the "*c*" direction of the unit cell, whereas in $AgTl_3I_5$ there are columns of the face-sharing octahedra that spread in the same direction. The crystal structure of $AgTl_2I_3$ represents an intermediate case, in which two tetrahedra and one octahedron share faces to form a finite fragment. The crystal structures of $AgTl_2I_3$ and $AgTl_3I_5$ feature additional iodine atoms not involved in the polyhedra around silver; moreover, in the latter structure part of these iodine atoms form the I–I dumbbells with the bond distance of 2.90 Å, which is typical for various metal polyiodides and iodide–iodine systems [9].

The ternary Ag–Tl–I system was investigated by several authors [10–12], mainly with respect to the AgI–TlI section. According to the literature [10] this section includes two ternary compounds $AgTl_2I_3$ and $AgTlI_2$ melting congruently at 600 K and incongruently by the peritectic reaction at 513 K, respectively. The eutectic compositions were found to be 70 and 27 mol% TlI at temperatures 590 and 475 K, respectively. Other sources [11,12] state that $AgTlI_2$ forms by the peritectoid reaction at 498–500 K, whereas $AgTl_2I_3$ melts congruently at 604 K. Also, the coordinates of eutectic points presented in the literature [10–12] are different. Our preliminary data [13] enabled us to refine accurately the T–x diagram of the quasi-binary AgI–TlI system (Fig. 2). The melting points of ternary compounds

* Corresponding author at: Z. Khalilov Str. 23, Baku, AZ 1148, Azerbaijan.
** Corresponding author at: Leninskie Gory 1-3, Moscow 119991, Russia.
E-mail addresses: babanly_mb@rambler.ru (M.B. Babanly), shev@inorg.chem.msu.ru (A.V. Shevelkov).

0925-8388/$ – see front matter © 2012 Elsevier B.V. All rights reserved.
doi:10.1016/j.jallcom.2012.02.051

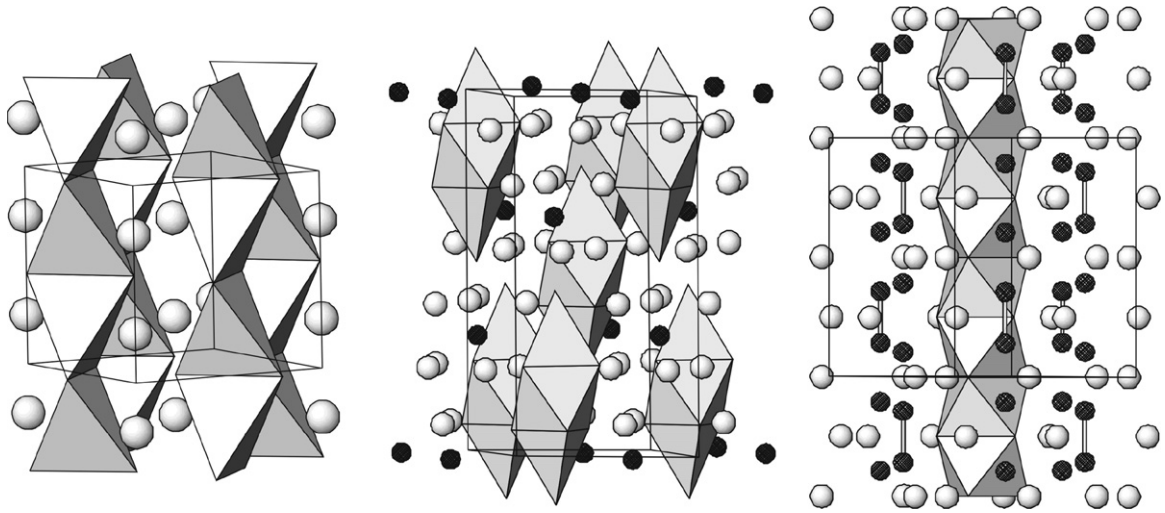

Fig. 1. Crystal structures of (from left to right) $AgTlI_2$, $AgTl_2I_3$, and $AgTl_3I_5$. Polyhedra around silver are shown. Thallium and iodine atoms are depicted as large gray and dark hatched spheres, respectively.

$AgTl_2I_3$ (603 K) and $AgTlI_2$ (510 K) as well as coordinates of eutectic compositions appeared to be very close to those presented in Ref. [10]. Moreover, X-ray powder diffraction study of alloys of the AgI–TlI system with 80 and 90 mol.% AgI quenched after annealing at 570 K did not confirm the literature assumption [11] about the existence of the η-phase in the temperature range of 478–633 K. Apparently, the specified alloys consisted of two-phase mixtures of AgI and $AgTlI_2$.

In our preliminary study of the AgI–TlI, Ag–TlI and Ag–$AgTl_2I_3$ polythermal sections [13], we found that the Ag–TlI and Ag–$AgTl_2I_3$ sections are quasi-binary and characterized by monotectic and eutectic type equilibriums, with a degenerate eutectic at the low-melting component side. Also, we constructed the T–x diagram of the Ag–AgI subsystem and internal sections Ag–$AgTlI_2$ and AgI–Tl of the Ag–AgI–TlI–Tl subsystem, as well as the projection of the liquidus surface of this subsystem (Fig. 3) [14]. It was shown that the subsystem is characterized by the immiscibility field in the liquid state. We found that the liquidus surface of the Ag–AgI–TlI–Tl system consists of six fields corresponding to primary crystallization of Ag, Tl, AgI, TlI, $AgTlI_2$ and $AgTl_2I_3$. The liquidus surface of all but the first phase is degenerated along the border systems AgI–TlI and TlI–Tl. The same is true for the non- and monovariant equilibriums, which are connected with them.

Considering the incompleteness and discrepancy of the literature data on phase equilibriums in the Ag–Tl–I system, we undertook the complete study of this system in all composition areas. Here, we report the result of the complex investigation of phase equilibriums in the AgI–TlI–I subsystem and thermodynamic properties of the ternary compounds in this subsystem. We took into account that the initial compounds AgI and TlI were studied in detail. AgI melts congruently at 828 K and has polymorphous transitions at 408 and 420 K, respectively [1,15]; however, the phase diagram of the binary Ag–I system is not given in the literature. The Tl–I system includes three binary compounds TlI, Tl_3I_4 and TlI_3. The former melts congruently at 715 K and has a polymorphous transition at 452 K; the other two phases melt incongruently by peritectic reactions at 533 and 403 K, respectively [16,17].

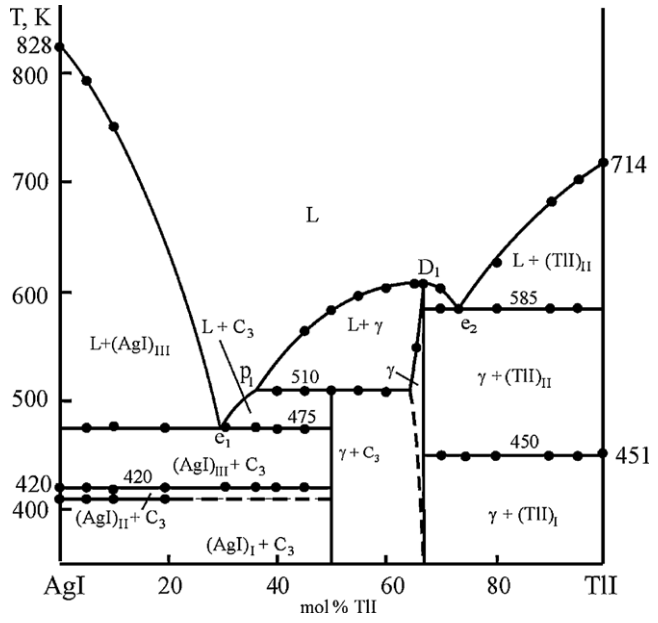

Fig. 2. Phase diagram of the quasi-binary AgI–TlI system according to Ref. [13].

2. Experimental

2.1. Synthesis

AgI, TlI, TlI_3 and Tl_3I_4 were synthesized from the elements of high purity grade in evacuated (~10^{-2} Pa) silica ampoules following a specially designed method which takes into account high volatility of iodine. The synthesis was performed in an inclined two-zone furnace, with the hot zone kept at a temperature 20–30 K higher than the corresponding melting point of a synthesized compound, whereas the temperature of the cold zone was about 400 K. After the main portion of iodine had reacted, the ampoule was relocated in such a manner that the product could melt at 850 K (AgI) or 750 K (TlI). The melt was stirred at this temperature by shaking the furnace and then cooled with the furnace. Due to the peritectic character of formation of compounds TlI_3 and Tl_3I_4 their syntheses were followed by annealing at 375 and 460 K, respectively, for 200 h.

Ternary compounds $AgTl_2I_3$, $AgTlI_2$, and $AgTl_3I_5$ were prepared using the same synthetic procedure. As a rule, the samples of the AgI–TlI–I system (total mass, 0.5 g) were prepared from the above-mentioned binary and ternary compounds. Considering high pressure of elementary iodine and TlI_3 the synthesis of most alloys was performed in thick-walled (4 mm) silica ampoules. Most of the alloys were annealed at 500 K for 1000 h, but samples containing TlI_3 and/or iodine were additionally annealed at 360 K for 500 h. In addition, Ag_4RbI_5 was synthesized from chemically pure RbI and AgI according to the procedure reported in the literature [18].

2.2. Analysis

X-ray powder diffraction (XRD) and differential thermal analysis (DTA) were used to analyze the samples. The XRD analysis was performed on a Bruker D8 ADVANCE diffractometer with Cu-$K\alpha_1$ radiation. The lattice parameters were refined using the TopasV3.0 software. For the DTA measurements, the NTR-72 device

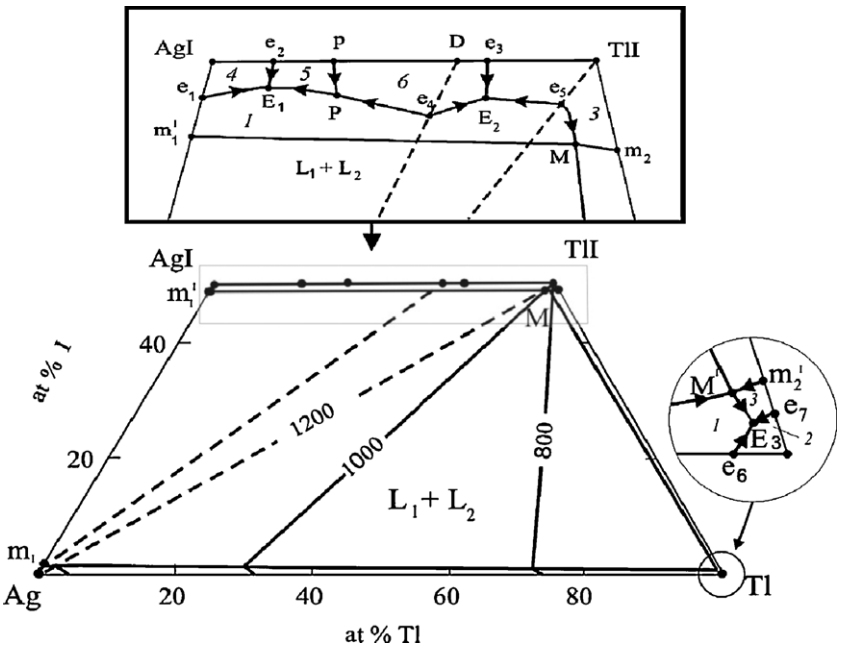

Fig. 3. Projection of the liquidus surface of the Ag–AgI–TlI–Tl system according to Ref. [14]. Primary crystallization fields are shown: 1, α (retrograde solid solutions in the Ag–Tl system); 2, Tl_{II}; 3, $(TlI)_{II}$; 4, $(AgI)_{III}$; 5, $AgTlI_2$; 6, $AgTl_2I_3$. Quasi-binary sections are shown with dashed lines.

equipped with two chromel–alumel thermocouples was used. The ramp rate was 5 K m^{-1}. Temperatures of thermal effects were taken mainly from the heating curves.

XRD confirmed that the pre-synthesized binary and ternary compounds were phase-pure, and that the unit cell parameters perfectly matched the literature data for all ternary compounds: $AgTlI_2$, $AgTl_2I_3$, and $AgTl_3I_5$ [6–8].

The melting points of pre-synthesized ternary compounds were measured and found to be in excellent agreement with the literature data.

2.3. EMF measurements

For the electro-motive force (EMF) measurements, the following concentration chains were assembled:

$$(-)\,AgI(solid)/Ag_4RbI_5(solid)/(Ag\ in\ alloys)(solid)(+) \quad (1)$$

In the chains of type (1), solid-state superionic conductor Ag_4RbI_5 was used as the electrolyte. This compound possesses high ion conductivity, $\sigma_i = 0.25\ \Omega^{-1}\ cm^{-1}$ at room temperature [12,19]. Ag_4RbI_5 melts at 503 K by a peritectic reaction, but below 300 K, it decomposes in the solid-state [1,2]. In the chains (1), AgI with the 0.01 at.% excess of iodine was used as the left electrode; the equilibrium alloys of the system with the desired composition were used as the right electrode. The electrodes were prepared by pressing the alloys in the form of pellets with the mass of 0.5 g.

The electrochemical cell described in detail elsewhere [20,21] was assembled and placed in a tubular furnace; temperature was stabilized at ~350 K for 40–50 h. EMF was measured by the compensation method in the temperature range of 300–360 K with the accuracy of ±0.1 mV, using the high-resistance universal B7-34A digital voltmeter. In each experiment the first reading was performed approximately 30 h after the start of the experiment, and then 4–5 h after reaching the desired temperature, which ensures the achievement of equilibrium. Considered equilibrium were the EMF readings that varied by no more than 0.5 mV regardless of the direction of the temperature change at repeated measurements at a given temperature. In order to eliminate the contribution of the thermopower, all contacts and leads were kept at the same temperature. The reversibility of the assembled concentration chains and the reproducibility of the results were controlled by checking the mass of the electrodes before and after the measurements and further confirmed by the chemical analysis of selected electrodes after the measurements. It was shown that the composition and mass of the electrodes remained constant during the experiment.

3. Results and discussion

The combined analysis of all our experimental data and the results found in the literature on the phase equilibriums in the Tl–I [17] and AgI–TlI (Fig. 2) systems allowed us to construct a self-consistent diagram of the phase equilibriums in the AgI–TlI–I subsystem of the Ag–Tl–I system. This subsystem includes all three ternary silver-thallium halides $AgTl_3I_5$ (C_1), $AgTl_2I_3$ (C_2), and $AgTlI_2$ (C_3).

3.1. Quasi-binary sections

It is established that the AgI–TlI–I subsystem has three quasi-binary sections. For the purpose of easy comparison, all the quasi- and non-quasi-binary polythermal sections are expressed using the normalized compositions, meaning that the number of atoms in initial components is equalized. The thermodynamic functions are expressed per mole of formula units.

3.1.1. The section $AgTl_3I_5$–4.5TlI

$AgTl_3I_5$–4.5TlI is a quasi-binary section of simple eutectic type (Fig. 4a). The eutectic composition lies at ~90 mol% $AgTl_3I_5$ and a temperature of 565 K. The polymorphous transition temperature of TlI (451 K) does not vary with changing composition that points to the insignificant compositional range of solid solutions based on this compound in the system $AgTl_3I_5$–4.5TlI.

3.1.2. The section $AgTl_3I_5$–1.5$AgTl_2I_3$

The section $AgTl_3I_5$–1.5$AgTl_2I_3$ (Fig. 4b) is characterized by the eutectic equilibrium which is found to be at 85 mol% $AgTl_3I_5$ and 562 K.

3.1.3. The section $AgTl_3I_5$–9I

The quasi-binary section $AgTl_3I_5$–9I is of monotectic type (Fig. 4c). At the monotectic temperature of 565 K, the immiscibility field ranges from ~5 to 95 mol% $AgTl_3I_5$. The eutectic contains approximately 3 mol% $AgTl_3I_5$ and crystallizes at 375 K.

XRD data confirm the phase diagrams of the above-mentioned systems. The XRD patterns for some alloys of the $AgTl_3I_5$–TlI system are presented in Fig. 5. It is clear that the diffractograms for all intermediate alloys display peaks of the initial compounds, meaning that these alloys are the mixtures of the boundary compositions. Intensity of the peaks varies with composition change according to the phase diagram. Similar diffraction patterns (not shown) are observed for other two systems.

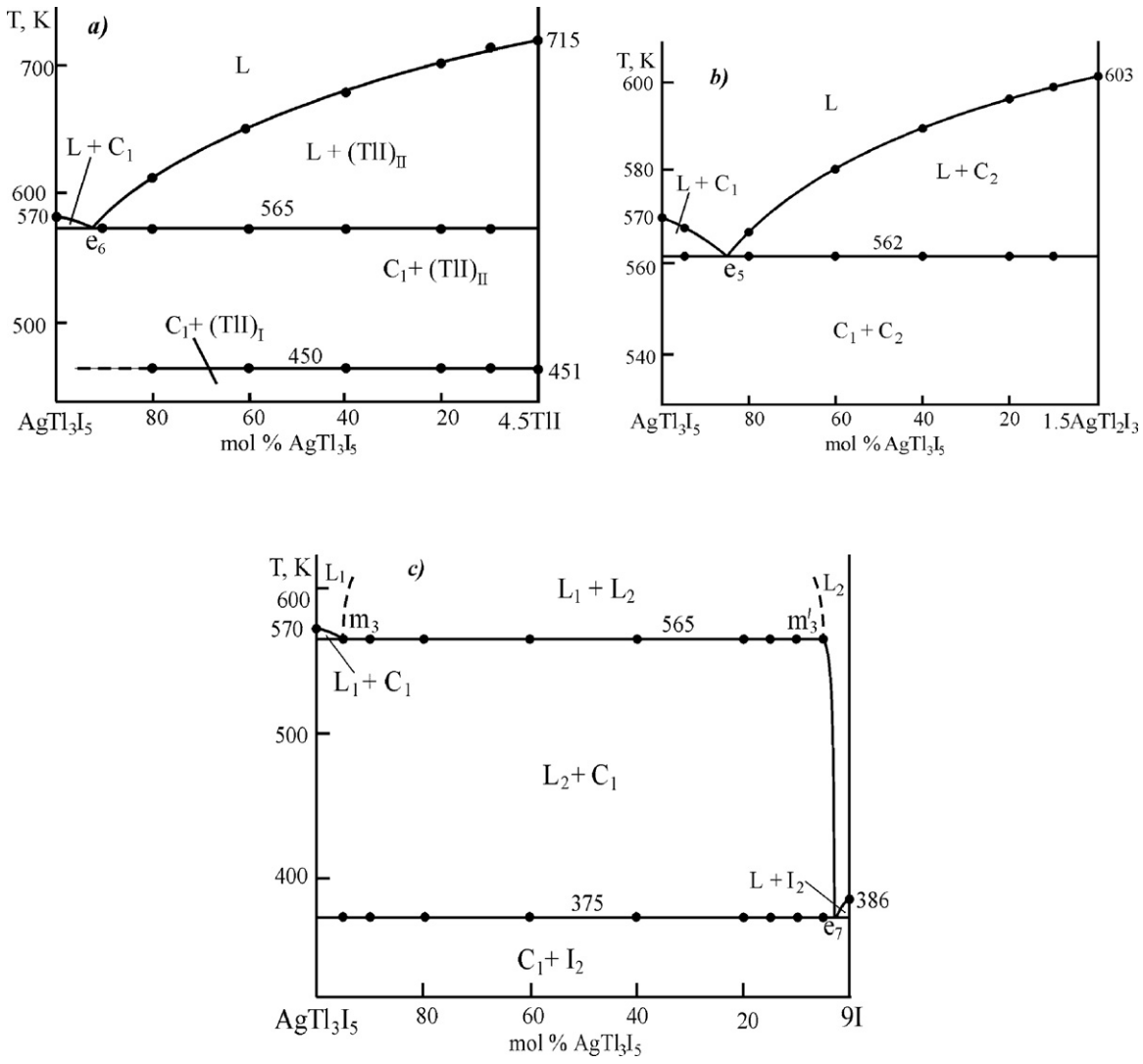

Fig. 4. Phase diagrams of the systems $AgTl_3I_5$–4.5TlI (a), $AgTl_3I_5$–1.5$AgTl_2I_3$ (b), and $AgTl_3I_5$–9I (c).

3.2. Non-quasi-binary polythermal sections

For easier comparison and better understanding, all non-quasi-binary polythermal sections (Figs. 6 and 7) will be discussed along with the projection of the liquidus surface (Fig. 8).

3.2.1. The section 7/9$AgTl_3I_5$–Tl_3I_4

The section 7/9$AgTl_3I_5$–Tl_3I_4 is a non-quasi-binary one due to the incongruent melting character of Tl_3I_4 [16]; however it is stable below the solidus (Fig. 6a). The liquidus surface is presented by two curves. The first one corresponds to primary crystallization

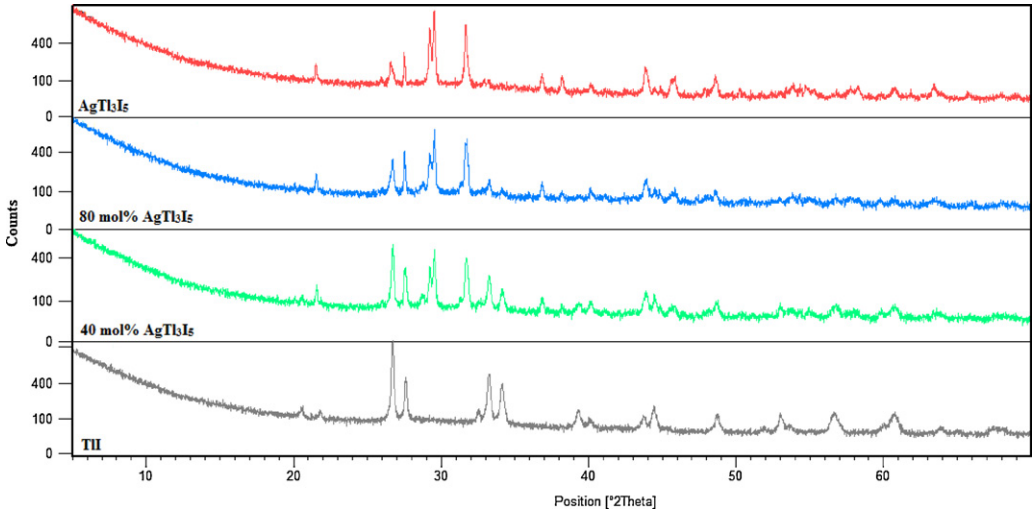

Fig. 5. XRD patterns of alloys of the $AgTl_3I_5$–TlI system.

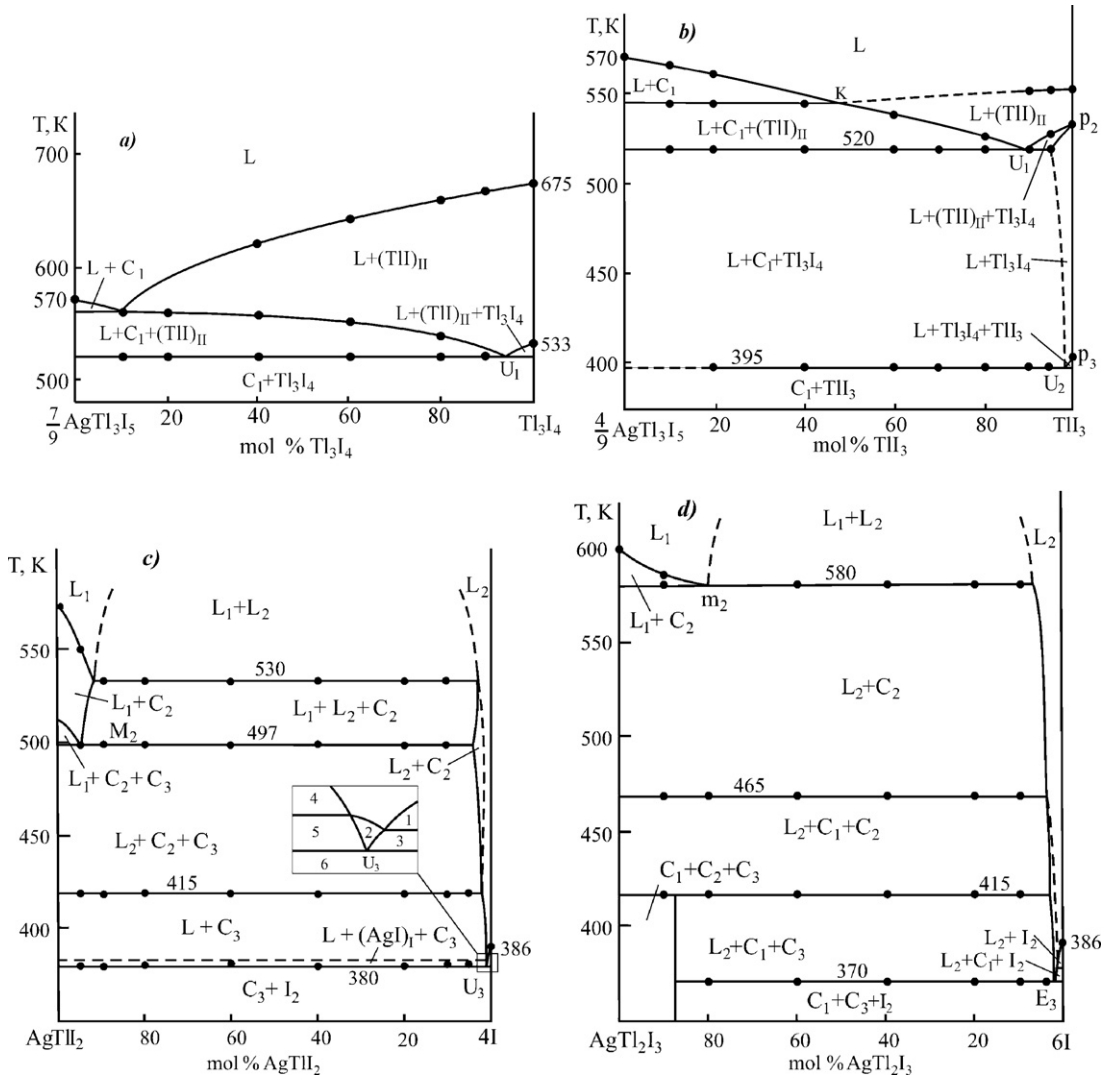

Fig. 6. Polythermal sections $7/9AgTl_3I_5$–Tl_3I_4 (a), $4/9AgTl_3I_5$–TlI_3 (b), $AgTlI_2$–4I (c), and $AgTl_2I_3$–6I (d) of the Ag–Tl–I system. Phase areas in (c): 1, L + I_2; 2, L + $(AgI)_I$; 3, L + $(AgI)_I$ + I_2; 4, L + C_3; 5, L + $(AgI)_I$ + C_3; 6, C_3 + I_2.

of $AgTl_3I_5$ (0–10 mol% Tl_3I_4) and the second one to primary crystallization of the high-temperature modification of thallium monoiodide $(TlI)_{II}$. Below the liquidus, secondary crystallization of phases proceeds by monovariant eutectic (2) or peritectic (3) reactions.

$$L \leftrightarrow AgTl_3I_5 + (TlI)_{II} \quad (560\text{–}520\,K;\ 0\text{–}95\,mol\%\,Tl_3I_4) \tag{2}$$

$$L + (TlI)_{II} \leftrightarrow Tl_3I_4 \quad (533\text{–}520\,K;\ 95\text{–}100\,mol\%\,Tl_3I_4) \tag{3}$$

Crystallization concludes by the invariant transition reaction at 520 K labeled U_1 (Fig. 8, Table 1):

$$L + (TlI)_{II} \leftrightarrow AgTl_3I_5 + Tl_3I_4 \tag{4}$$

3.2.2. The section $4/9AgTl_3I_5$–TlI_3

The section $4/9AgTl_3I_5$–TlI_3 is also non-quasi-binary (Fig. 6b) due to the incongruent melting of TlI_3 [16]. Compounds $AgTl_3I_5$ (0–50 mol% TlI_3) and $(TlI)_{II}$ primarily crystallize from the melt. The horizontal line at 545 K and the curve KU_1 correspond to a joint crystallization of these phases by the eutectic reaction (2). The peritectic reaction (3) occurs in the composition range ~95–100 mol% TlI_3. The invariant transition reaction (4) occurs at 520 K. The crystallization process in this system finishes with the following transition reaction (U_2 in Fig. 8 and Table 1):

$$L + Tl_3I_4 \leftrightarrow AgTl_3I_5 + TlI_3 \tag{5}$$

3.2.3. The sections $AgTlI_2$–4I and $AgTl_2I_3$–6I

The sections $AgTlI_2$–4I (Fig. 6c) and $AgTl_2I_3$–6I (Fig. 6d) are characterized by a wide immiscibility field of two liquid phases ($L_1 + L_2$) and the primary crystallization of the $AgTl_2I_3$ compound from this field. The horizontal line at 497 K in Fig. 6c corresponds to the invariant monotectic equilibrium M_2, whereas the horizontal line at 415 K corresponds to the decomposition process by the transition reaction U_4 (Fig. 8, Table 1). The $AgTl_2I_3$–6I section looks like a quasi-binary system of monotectic type above 465 K. Below this temperature joint crystallization of $AgTl_2I_3$ and $AgTl_3I_5$ starts. At the end of this process the compound $AgTl_3I_5$ decomposes by the transition reaction U_4 (415 K). The crystallization process concludes by the transition reaction (U_3) within the $AgTlI_2$–4I section and by the eutectic reaction (E_3) within the $AgTl_2I_3$–6I section.

3.2.4. The section 2AgI–TlI_3

The section 2AgI–TlI_3 is characterized by more complicated interactions and shows more heterogeneous equilibriums of the system (Fig. 7). In this section, the invariant monotectic (M_1, M_2,

Table 1
Invariant equilibriums in the AgI–TlI–I system.

Point on Fig. 8	Equilibrium	Composition, at.%		T, K
		Tl	I	
D_1	$L \leftrightarrow AgTl_2I_3$	33.3	50	603
D_2	$L \leftrightarrow AgTl_3I_5$	33.3	55.5	570
p_1	$L + AgTl_2I_3 \leftrightarrow AgTlI_2$	18.7	50	510
p_2	$L + (TlI)_{II} \leftrightarrow Tl_3I_4$	22	78	535
p_3	$L + Tl_3I_4 \leftrightarrow TlI_3$	16	84	402
U_1	$L + (TlI)_{II} \leftrightarrow Tl_3I_4 + AgTl_3I_5$	20.5	78	520
U_2	$L + Tl_3I_4 \leftrightarrow TlI_3 + AgTl_3I_5$	15	84	395
U_3	$L + (AgI)_I \leftrightarrow AgTlI_2 + I_2$	–	>98	380
U_4	$L + AgTl_2I_3 \leftrightarrow AgTlI_2 + AgTl_3I_5$	~2	~97	415
e_1	$L \leftrightarrow (AgI)_{III} + AgTlI_2$	13	50	475
e_2	$L \leftrightarrow (TlI)_{II} + AgTl_2I_3$	36	50	585
e_3	$L \leftrightarrow TlI_3 + I_2$	12	88	363
e_4	$L \leftrightarrow (AgI)_I + I_2$	–	>99	385
e_5	$L \leftrightarrow AgTl_2I_3 + AgTl_3I_5$	34	54.5	562
e_6	$L \leftrightarrow (TlI)_{II} + AgTl_3I_5$	35.5	55.2	565
e_7	$L \leftrightarrow AgTl_3I_5 + I_2$	~1.5	~98	375
E_1	$L \leftrightarrow AgTl_2I_3 + AgTl_3I_5 + (TlI)_{II}$	35	54	560
E_2	$L \leftrightarrow AgTl_3I_5 + TlI_3 + I_2$	11.5	87.5	360
E_3	$L \leftrightarrow \leftrightarrow AgTlI_2 + AgTl_3I_5 + I_2$	–	>98	370
$m_1(m_1')$	$L_1 \leftrightarrow L_2 + (AgI)_{III}$	–	~50.5(>99)	825
$m_2(m_2')$	$L_1 \leftrightarrow L_2 + AgTl_2I_3$	30	55(>97)	580
$m_3(m_3')$	$L_1 \leftrightarrow L_2 + AgTl_3I_5$	31.5	58(>97)	565
$M_1(M_1')$	$L_1 \leftrightarrow L_2 + (AgI)_{III} + AgTlI_2$	14(<1)	52(>99)	465
$M_2(M_2')$	$L_1 + AgTl_2I_3 \leftrightarrow L_2 + AgTlI_2$	18.5(<1)	52.5(>98)	497
$M_3(M_3')$	$L_1 \leftrightarrow L_2 + AgTl_2I_3 + AgTl_3I_5$	31(<1)	56(>97)	555

M_3, m_2, m_3), transition (U_1–U_4) and eutectic (E_2, E_3, e_7) equilibriums are clearly seen. Comparison of Fig. 7 with Fig. 8 and Table 1 allows establishing types of equilibriums expressed by the curves M_1M_2, M_2M_3, U_1U_2, e_7E_2 and some others. In this section, the transition reaction (U_4) describing the decomposition of $AgTl_2I_3$ into $AgTlI_2$ and $AgTl_3I_5$ (horizontal line at 415 K) and polymorphous transition of AgI at 420 K and 410 K are explicitly shown. Below the solidus the AgI–TlI_3 section intersects three three-phase fields $(AgI)_I + AgTlI_2 + I_2$, $AgTl_3I_5 + AgTlI_2 + I_2$ and $AgTl_3I_5 + TlI_3 + I_2$.

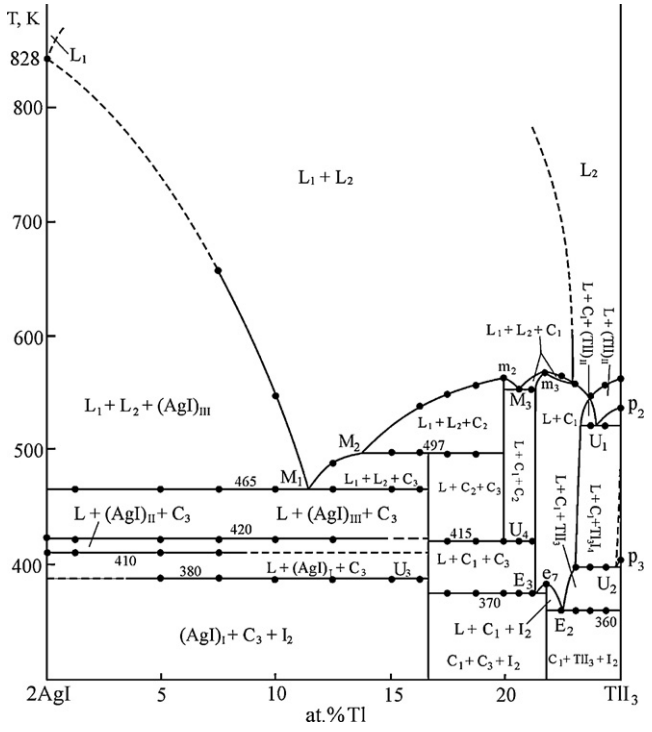

Fig. 7. Polythermal section 2AgI–TlI_3 of the Ag–Tl–I system.

3.3. The liquidus surface of the AgI–TlI–I system

The liquidus surface of the AgI–TlI–I system consists of eight fields corresponding to the primary crystallization of the four binary and three ternary compounds and elemental iodine (Fig. 8). The characteristic feature of this system is the presence of a wide immiscibility field within the border system AgI–I_2. This field spreads over slightly more than 75% of the system and covers primary crystallization areas of all ternary phases: $AgTlI_2$, $AgTl_2I_3$, and $AgTl_3I_5$. Subsequently, peritectic (p_1) and eutectic (e_1 and e_2) curves pass through this field and transform quadriphase monotectic equilibriums M_1, M_2 and M_3 (Fig. 8).

The types and coordinates of invariant equilibriums are listed in Table 1. Herein also are presented the invariant equilibriums of border systems and quasi-binary sections of the ternary system AgI–TlI–I. Some invariant and monovariant equilibriums are degenerated at the elemental iodine side. Schematic descriptions of this area are given in Fig. 8 as blow-ups. The corresponding invariant equilibriums are listed in Table 1.

Quasi-binary sections and ties in the subsolidus are shown as dashed lines in Fig. 8. The AgI–TlI–I system consists of seven three-phase fields in the subsolidus.

3.4. Thermodynamic functions

The results of the EMF measurements for the chains of type (1) not only allowed confirming the correctness of all drawn solid-state equilibriums but also served as the basis for the calculation of the thermodynamic functions for $AgTlI_2$, $AgTl_2I_3$ and $AgTl_3I_5$.

The analysis showed the linearity of the EMF dependences on temperature for various alloys of the heterogeneous subsystems AgI–TlI–I. Accordingly, the linear least-squares treatment of the data was performed [22] and the results were expressed according to the literature recommendations [23] as

$$E, mV = a + bT \pm t\left[\frac{S_E^2}{n} + S_b^2(T - \overline{T})^2\right]^{1/2} \quad (6)$$

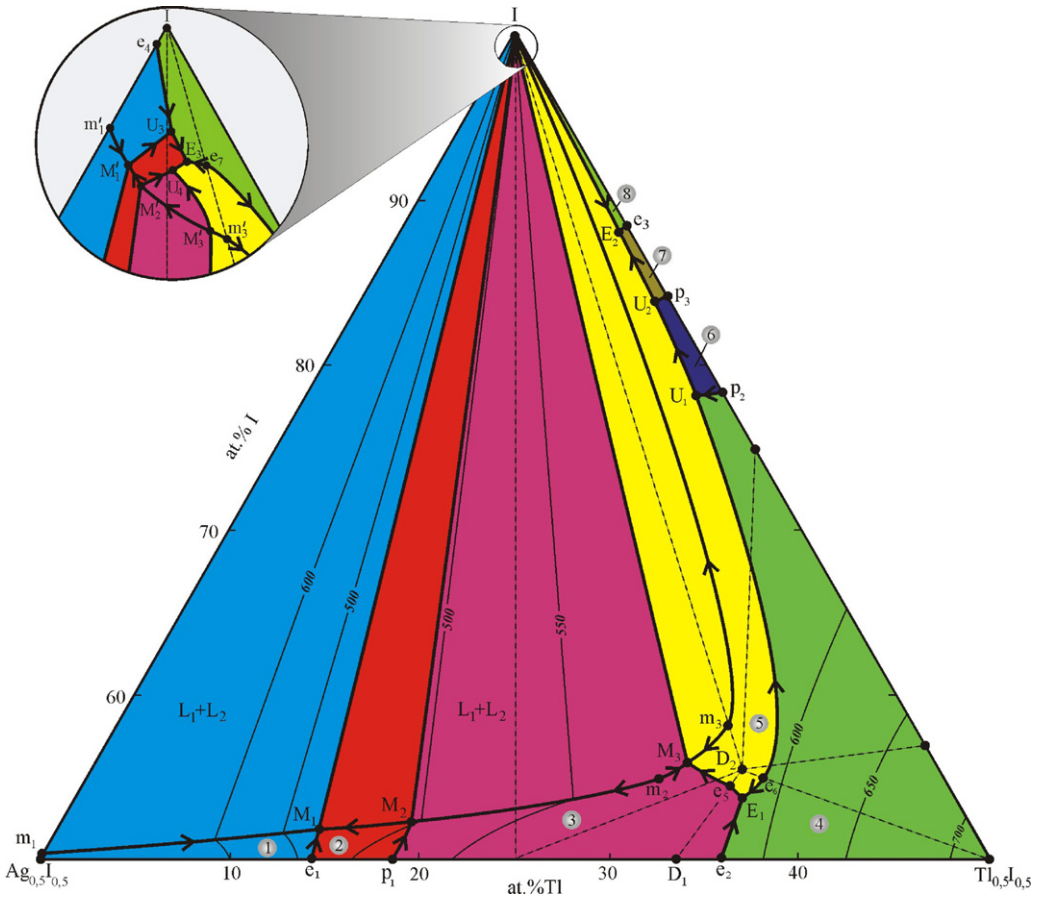

Fig. 8. Projection of the liquidus surface of the Ag–AgI–TlI–Tl system. Primary crystallization fields are shown: 1, $(AgI)_{III}$; 2, $AgTlI_2$ (C_3); 3, $AgTl_2I_3$ (C_2); 4, $(TlI)_{II}$; 5, $AgTl_3I_5$ (C_1); 6, Tl_3I_4; 7, TlI_3; 8, I_2. Quasi-binary and stable sections in the subsolidus area are shown with dashed lines.

where n is the number of pairs of E and T values; S_E and S_b are the error variances of the EMF readings and b coefficient, respectively; $\overline{T}$ is the mean absolute temperature; and t is the Student's test. At the confidence level of 95% and $n \geq 20$, the Student's test is $t \leq 2$ [21,22]. By using received equations of type (6) (Table 2) and following thermodynamic expressions [21]

$$\Delta\overline{G}_{AgI} = -zFE$$

$$\Delta\overline{H}_{AgI} = -zFa$$

$$\Delta\overline{S}_{AgI} = zFb$$

the partial molar functions of silver iodide in the alloys ($\Delta\overline{Z}_{AgI} = \Delta\overline{G}_{AgI}$; $\Delta\overline{H}_{AgI}$; $\Delta\overline{S}_{AgI}$) were calculated at 298 K. The results are listed in Table 3. These functions express the difference between the partial molar thermodynamic functions of silver in the AgI–TlI–I alloys ($\Delta\overline{Z}_{Ag}$) and in pure silver monoiodide ($\Delta\overline{Z}'_{Ag}$): $\Delta\overline{Z}_{AgI} = \Delta\overline{Z}_{Ag} - \Delta\overline{Z}'_{Ag}$ On the other hand, silver iodide is the only compound in the binary Ag–I system and its homogeneity range is undetectable. Therefore $\Delta\overline{Z}'_{Ag}$ are the thermodynamic functions of the following reaction [21]:

$$Ag(solid) + 1/2I_2(solid) \rightarrow AgI(solid)$$

i.e. $\Delta\overline{Z}'_{Ag} = \Delta_f Z^0(AgI)$. Then the partial molar functions of silver in the alloys of the AgI–TlI–I system can be calculated as

$$\Delta\overline{Z}_{Ag} = \Delta_f Z^0(AgI) + \Delta\overline{Z}_{AgI} \quad (7)$$

The obtained values are listed in Table 4.

According to the phase diagram of the AgI–TlI–I system, the partial molar functions of silver in this subsystem are thermodynamic functions of the following potential-forming reactions (all substances are solid) [21]:

$$Ag + 0.8Tl_3I_4 + 0.6TlI_3 = AgTl_3I_5$$

$$Ag + TlI + AgTl_3I_5 = 2AgTl_2I_3$$

Table 2
Temperature dependences of the EMF for the chains of type (1) for alloys of the AgI–TlI–I in the temperature range of 300–360 K.

Phase area	E, mV = $a + bT \pm 2S_E(T)$
$AgTl_3I_5 + Tl_3I_4 + TlI_3$	$67.52 + 0.354 \pm 2\left[\frac{21.2}{25} + 1.3 \cdot 10^{-3}(-344.3)^2\right]^{1/2}$
$AgTlI_2 + AgTl_3I_5 + I_2$	$46.39 + 0.0465 \pm 2\left[\frac{8.9}{24} + 5.6 \cdot 10^{-4}(-345.3)^2\right]^{1/2}$
$AgTl_2I_3 + TlI + AgTl_3I_5$	$79.34 + 0.188 \pm 2\left[\frac{5.5}{24} + 3.4 \cdot 10^{-4}(-346.7)^2\right]^{1/2}$

Table 3
Relative partial thermodynamic functions of AgI in the alloys of the AgI–TlI–I system at 298 K.

Phase area	$-\Delta\overline{G}_{AgI}$	$-\Delta\overline{H}_{AgI}$	$\Delta\overline{S}_{AgI}$ J K^{-1} mol^{-1}
	kJ mol^{-1}		
$AgTl_3I_5 + Tl_3I_4 + TlI_3$	16.70 ± 0.39	6.51 ± 2.43	34.16 ± 7.05
$AgTlI_2 + AgTl_3I_5 + I_2$	5.81 ± 0.24	4.48 ± 1.58	4.49 ± 4.55
$AgTl_2I_3 + TlI + AgTl_3I_5$	13.06 ± 0.19	7.65 ± 1.24	18.14 ± 3.56

Table 4
Relative partial thermodynamic functions of silver in the alloys of the AgI–TlI–I system at 298 K.

Phase area	$-\Delta\overline{G}_{Ag}$	$-\Delta\bar{H}_{Ag}$	$\Delta\overline{S}_{Ag}$ J K^{-1} mol^{-1}
	kJ mol^{-1}		
$AgTl_3I_5 + Tl_3I_4 + TlI_3$	83.06 ± 0.45	68.45 ± 2.81	49.00 ± 4.10
$AgTlI_2 + AgTl_3I_5 + I_2$	72.17 ± 0.29	66.42 ± 1.96	19.30 ± 5.82
$AgTl_2I_3$ + TlI + $AgTl_3I_5$	79.42 ± 0.24	69.59 ± 1.62	32.96 ± 4.86

Table 5
Standard integral thermodynamic functions of compounds in the AgI–TlI–I system at 298 K.

Compound	$-\Delta_f G^0$(298 K)	$-\Delta_f H^0$(298 K)	S^0(298 K) J K^{-1} mol^{-1}
	kJ mol^{-1}		
AgI [25]	66.36 ± 0.05	61.94 ± 0.38	115.48 ± 1.26
TlI [25]	125.31 ± 0.33	123.69 ± 0.42	127.70 ± 0.21
Tl_3I_4 [24]	404.73 ± 2.04	392.2 ± 6.5	466.9 ± 20.1
TlI_3 [24]	142.79 ± 0.73	135.4 ± 2.9	263.3 ± 7.4
$AgTl_3I_5$	492.52 ± 2.52	463.4 ± 9.7	623.1 ± 24.5
$AgTlI_2$	212.29 ± 1.03	198.8 ± 4.6	268.3 ± 12.1
$AgTl_2I_3$	348.63 ± 1.55	328.4 ± 5.9	413.1 ± 14.8

$$Ag + 0.5AgTl_3I_5 + 0.25I_2 = 1.5AgTlI_2 \quad (8)$$

Using these equations, the standard thermodynamic functions of formation for the above-mentioned ternary compounds can be exactly calculated from the data presented in Table 4 and appropriate functions of TlI, Tl_3I_4 and TlI_3. For example, we can calculate the integral thermodynamic functions of formation of $AgTl_3I_5$ as

$$\Delta_f Z^0(AgTl_3I_5) = \Delta\bar{Z}_{Ag} + 0.8\Delta_f Z^0(Tl_3I_4) + 0.6\Delta_f Z^0(TlI_3) \quad (9)$$

where $\Delta\overline{Z}_{Ag}$ is the partial thermodynamic function ($\Delta\overline{G}_{Ag}$ $\Delta\overline{H}_{Ag}$) of silver; $\Delta_f Z^0_{Tl_3I_4}$ and $\Delta_f Z^0_{TlI_3}$ are the standard thermodynamic functions of formation of Tl_3I_4 and TlI_3, respectively. The standard entropy of $AgTl_3I_5$ was calculated using the following equation:

$$S^0(AgTl_3I_5) = \overline{\Delta S}_{Ag} + S^0(Ag) + 0.8S^0(Tl_3I_4) + 0.6S^0(TlI_3) \quad (10)$$

The standard integral thermodynamic functions of the compounds $AgTl_2I_3$ and $AgTlI_2$ were calculated in a similar way. The results of calculations are presented in Table 5. For the calculations, the thermodynamic parameters of Tl_3I_4 and TlI_3 were taken from the literature [24] and the thermodynamic parameters of AgI and TlI as well as the standard entropy (S^0_{298}) of silver were taken from the database [25] (see Table 5). In all cases the estimated standard deviations were calculated by accumulation of errors.

4. Conclusions

Application of various experimental methods, including DTA, XRD, and EMF analysis, enabled us to build the self-consistent phase diagram of the AgI–TlI–I system. This system is characterized by the wide immiscibility field within the border system AgI–I_2 which occupies slightly more than 75% of the ternary system and covers primary crystallization areas of $AgTlI_2$, $AgTl_2I_3$ and $AgTl_3I_5$. The partial molar functions of silver iodide and silver in alloys, as well as standard thermodynamic functions of formation and standard entropies of $AgTlI_2$, $AgTl_2I_3$ and $AgTl_3I_5$ were calculated from the EMF measurements and proved to be accurate.

Acknowledgment

This work was supported by the Science Development Foundation of the President of the Republic of Azerbaijan, grant no. EIF-2011-1(3)-82/69/4.

References

[1] A.K. Ivanov-Shits, I.V. Murin, Solid State Ionics, vol. 1, Saint-Petersburg University Publ., Saint-Petersburg, 2000.
[2] P. Hagenmüller, W. Van Goll (Eds.), Solid Electrolytes, Academic Press, New York, San Francisco, London, 1978.
[3] J.C. Burbano, R.A. Vargas, D. Peña-Lara, C.A Z. Lozano, H. Correa, Solid State Ionics 180 (2009) 1553–1557.
[4] B. Klimensz, T. Gorecki, C. Gorecki, Thermochim. Acta 374 (2001) 145–149.
[5] O.S. Oleneva, M.A. Kirsanova, T.A. Shestimerova, N.S. Abramchuk, D.I. Davliatshin, M.A. Bykov, E.V. Dikarev, A.V. Shevelkov, J. Solid State Chem. 181 (2008) 37–44.
[6] M. Hoyer, H. Hartl, Z. Anorg. Allg. Chem. 622 (1996) 308–312.
[7] P. Messien, Bulletin de la Société Royal des Sciences de Liège 38 (1969) 490–502.
[8] W. Stoeger, A. Rabenau, Z. Naturforsch. 33 (1978) 740–744.
[9] P.H. Svensson, L. Kloo, Chem. Rev. 103 (2002) 1203–1209.
[10] L.Q. Berg, I.N. Lepeshkov, News of Phys. Chem. Analysis sector IONX AN SSSR 15 (1947) 148.
[11] J.W. Brightwell, L.S. Miller, A. Munday, B. Ray, Phys. Stat. Sol. (a) 79 (1983) 293–300.
[12] J.N. Bradley, P.D. Green, Trans. Faraday Soc. 63 (1967) 424–430.
[13] L.F. Mashadieva, M.B. Babanly, Sci. Rep. Azerb. Techn. Univ. 1 (37) (2011) 102–105.
[14] L.F. Mashadieva, M.B. Babanly, U.A. Kulieva, News Baku State Univ. 1 (2011) 11–16.
[15] R.F. Rolsten, Iodide Metals and Metal Iodides, John Wiley and Sons, New York, 1961.
[16] T.B. Massalski (Ed.), Binary Alloy Phase Diagrams, 2nd ed., ASM International, Materials Park, Ohio, 1990.
[17] D. Cubicciotti, J. Less-Common Met. 24 (1971) 201–209.
[18] A.R. West, Solid State Chemistry and Its Applications, John Wiley and Sons, New York, 1984.
[19] B.B. Owens, G.R. Argue, Science 157 (1967) 308.
[20] M.B. Babanly, L.F. Mashadieva, G.M. Velieva, S.Z. Imamalieva, Yu.M. Shykhyev, Russ. J. Electrochem. 45 (2009) 399–404.
[21] M. Babanly, Y. Yusibov, N. Babanly, in: S. Kara (Ed.), Electromotive Force and Measurement in Several Systems, Intechweb.Org, 2011, pp. 57–78, ISBN 978-953-307-728-4.
[22] K. Doerffel, Statistik in der analytischen Chemie, Grundstoffindustrie, Leipzig, 1990.
[23] A.N. Kornilov, L.B. Stepina, V.A. Sokolov, J. Phys. Chem. 46 (1972) 2975–2979.
[24] L.F. Mashadieva, M.B. Babanly, Scientific reports of Azerb. Techn. Univ. 3 (2011) 122–125.
[25] Data base of thermal constants of substances, Digital version, In: V.S. Yungman (Ed.), 2006, http://www.chem.msu.ru/cgi-bin/tkv.